Signal Processing 96 (2014) 253–260

Contents lists available at ScienceDirect

Signal Processing

journal homepage: www.elsevier.com/locate/sigpro

Robust adaptive beamforming using an iterative FFT algorithm

Kai Yang [a,b], Zhiqin Zhao [a,*], Jiazhou Liu [a,b], Qing Huo Liu [b]

[a] School of Electronic Engineering, University of Electronic Science and Technology of China (UESTC), Chengdu 611731, China
[b] Department of Electrical and Computer Engineering, Duke University, Durham, NC 27708, USA

ARTICLE INFO

Article history:
Received 5 March 2013
Received in revised form
11 July 2013
Accepted 5 September 2013
Available online 13 September 2013

Keywords:
Robust adaptive beamforming
Peak sidelobe level
Power pattern synthesis
Iterative FFT

ABSTRACT

Adaptive beamformers will degrade in the presence of model mismatch. Because a wider beamwidth has higher ability against steering vector errors, and lower sidelobe levels can improve the robustness against fast moving interferences, in this work an iterative fast Fourier transform (FFT) based adaptive beamformer is proposed with constraints on beamwidth and peak sidelobe level. The adaptive beamforming is transformed to a weighted pattern synthesis problem. This weighted pattern is a product of the array pattern and a weighting function. Because the weighting function has shape peaks at the direction of interferences, it will have nulls in the array pattern at the directions of interferences by reducing the peak sidelobe level of this weighted pattern. A modified iterative FFT algorithm is proposed to synthesize this weighted pattern. Thanks to the efficiency of FFT, the nonconvex problem of power pattern synthesis can be solved efficiently. This method is demonstrated through several simulation examples. The results show the advantages of the proposed method in obtaining high output SINRs against moving target signals and steering vector errors.

1. Introduction

Adaptive beamforming has a wide range of applications in radar, sonar, wireless communications, medical imaging and other fields. The minimum variance distortionless response (MVDR) beamformer has superior interference rejection capability compared with the data-independent beamformers as long as the array model is known accurately [1]. In real world applications, model mismatch which can be caused by steering direction errors, imperfect array calibration, small sample size, the presence of desired signal component in the training data etc., are usually unavoidable. These imperfections will cause steering vector errors and interference-plus-noise covariance matrix cannot be estimated accurately. The performance of adaptive beamformers degrades with these imperfections. Thus, various robust adaptive beamforming techniques have been proposed in the past decades ([2–21], and many references therein). One popular and very effective approach to process the steering vector error is based on the principle of worst-case performance optimization [4]. This approach requires the steering vector error upper bound which is not known in many real world applications. Since the interference-plus-noise covariance matrix is unavailable in practice, it is usually replaced by the sample covariance matrix derived from received samples of the array output. However, the output signal-to-interference-plus-noise ratio (SINR) of MVDR beamformers with sample covariance matrix will be far from the optimal ones at the high SNRs when there is mismatch between the actual and presumed signal steering vectors or the number of snapshots is relatively small. Aiming to solve this problem, [12] proposed a robust adaptive beamforming method based on interference covariance matrix reconstruction. The output SINRs of the method in [12] are always close to optimal ones in a very large range of SNR when the array model is exactly known. However, this algorithm cannot control the beamwidth and the sidelobe levels.

* Corresponding author. Tel.: +86 28 61830698.
E-mail address: zqzhao@uestc.edu.cn (Z. Zhao).

0165-1684/$ - see front matter © 2013 Elsevier B.V. All rights reserved.
http://dx.doi.org/10.1016/j.sigpro.2013.09.003

If there are desired sources moving so fast that the array weights are unable to adapt fast enough, one may prefer to design an array beampattern with constant magnitude over a wide angle region. However, the beamforming with pattern magnitude constraints is a non-convex problem which is very time consuming. For a uniform linear array, this problem can be transformed into a convex problem with the transformation from the array output power and the magnitude response to linear functions of the autocorrelation sequence of the array weight [14,16]. Because the magnitude response is not smaller than 0 at all angles in $[0, 2\pi]$, enough inequality constraints on the magnitude response of different angels should be added in the optimization process (i.e. K in equation (21) of [14] should be large). If the number of sampling angles is small, the optimized autocorrelation sequence may not be an autocorrelation sequence at all. This makes this kind of technique have higher computational complexity compared with conventional robust adaptive beamforming, especially when the array is large. Most existing robust adaptive beamformers do not consider the sidelobe of the beampattern. If the beampattern has high sidelobes, it will degrade the performance greatly during the time interval of updating the weights when new interferences suddenly appear [18]. A second-order cone programming approach in [18] was proposed to control the sidelobe levels. However, this method did not consider the steering vector error which can severely degrade the performance.

An easy and promising iterative fast Fourier transform (FFT) method [22,23] was presented to synthesize large planar arrays, and it was later extended to synthesize nonuniform arrays [24] and uniform planar arrays with flat-top pattern [25]. This method is based on the Fourier transform-pair relationship between the array excitations and the array factor. Due to the efficiency of FFT, this method can solve large array synthesis problems efficiently. Here, we modify this iterative FFT method to optimize the weights of uniform linear arrays for power pattern synthesis.

In this paper, we will propose a robust adaptive beamformer based on a modified iterative FFT method for uniform linear arrays which can combine with constraints on the mainlobe beamwidth and sidelobe levels. First, we transfer the adaptive beamforming problem into a weighted array pattern synthesis problem, where the weighted pattern is a product of the array pattern and a weighting function. The value of the weighting function is equal to the Capon spectrum in the sidelobe area and is equal to a small constant in the mainlobe area. Therefore, for the weighting function, there are peaks at the directions of interferences and no peak at the direction of the target signal. Minimizing the output power of interferences and noise will be equal to minimizing the sidelobe levels of this weighted pattern. When we decrease the peak sidelobe level of the weighted pattern, the interferences are suppressed with high priority due to the great values of the weighting function at their direction of arrivals. Meanwhile we restrict the array has nearly constant magnitude response in a range of directions, which can improve the robustness of the beamformer against array steering vector errors. We adjust the array pattern by a modified iterative FFT method according to a weighted array pattern. When the weighted pattern is arrived at the desired one, the interferences have been suppressed and the array pattern satisfies the given constraints. Finally, the proposed method is validated by some simulation cases.

2. The proposed robust adaptive beamforming

Consider a uniform linear array with N isotropic sensors equally spaced at distance d that receives signals from multiple narrowband sources. The observation signal vector $\boldsymbol{x}(t)$ at the time instant t is an $N\times 1$ vector given as

$$\boldsymbol{x}(t)=\boldsymbol{s}(t)\boldsymbol{a}(u_o)+\boldsymbol{v}(t) \tag{1}$$

where $\boldsymbol{s}(t)$ is the waveform of the desired signal, $\boldsymbol{a}(u)=[1,e^{j2\pi du/\lambda},\ \ldots,\ e^{j2\pi(N-1)du/\lambda}]^T$, $u=\sin(\theta)$, u_o is associated with the target signal impinging on the array from direction θ_o, $\boldsymbol{v}(t)$ denotes the sum of the interferences and the noise. The output of beamformer is given as $\boldsymbol{y}(t)=\boldsymbol{w}^H\boldsymbol{x}(t)$, where $\boldsymbol{w}$ is the $N\times 1$ complex weight vector and $(\bullet)^H$ stands for the Hermitian transpose.

The goal of an adaptive beamformer is to receive the desired signal and reject the interferences as well as noise. With MVDR beamformer, the optimal weight vector $\boldsymbol{w}$ can be obtained by solving the following problem

$$\min_{w}\ \boldsymbol{w}^H\boldsymbol{R}_{\boldsymbol{v}}\boldsymbol{w}\ \text{subject to}\ \boldsymbol{w}^H\boldsymbol{a}(u_o)=1 \tag{2}$$

where $\boldsymbol{R}_v=E\{\boldsymbol{v}(t)\boldsymbol{v}^H(t)\}$ is the interference-plus-noise covariance matrix. The beamformer based on (2) is sensitive to the steering vector error which can come from direction of arrival mismatch, array calibration errors etc. To make the beamformer more robust to steering vector error, we constrain the array pattern gain over a wide direction range to be greater than a given constant. Moreover, we maintain low sidelobes against unexpected interferences. The problem (2) can be rewritten as

$$\min_{w}\ \boldsymbol{w}^H\boldsymbol{R}_v\boldsymbol{w} \tag{3a}$$

$$\text{subject to}\ \eta\le|\boldsymbol{w}^H\boldsymbol{a}(u)|\le 1,\ u\in U_m \tag{3b}$$

$$|\boldsymbol{w}^H\boldsymbol{a}(u)|\le\varepsilon,\ u\in U_s \tag{3c}$$

where η and ε are given constants representing the ripple level in the mainlobe and the peak sidelobe level in the sidelobe region, U_m and U_s represent the set of u in the mainlobe region and sidelobe region, respectively.

The constraint (3b) is non-convex which is time consuming to solve. In [14], by changing the variables $\boldsymbol{w}$ into the variables $\boldsymbol{r}$ which is defined as the autocorrelation sequence of complex weights, the non-convex constraints are transformed to convex ones. However, as Section 3.4 will show, the number of angular samples should be large enough to guarantee the variable $\boldsymbol{r}$ is an autocorrelation sequence. This will increase the computational complexity especially for the large arrays. In the following, we will propose a modified iterative FFT based method to solve (3a)–(3c) efficiently.

Since the interference-plus-noise covariance matrix $\boldsymbol{R}_v$ is unavailable in practice, we reconstruct $\boldsymbol{R}_v$ as [12]

$$\hat{\boldsymbol{R}}_v = \int_{U_s} \frac{\boldsymbol{a}(u)\boldsymbol{a}^H(u)}{\boldsymbol{a}^H(u)\hat{\boldsymbol{R}}_x^{-1}\boldsymbol{a}(u)} du \tag{4}$$

where $\hat{\boldsymbol{R}}_x$ represents the sample covariance matrix which is given by

$$\hat{\boldsymbol{R}}_x = \frac{1}{T}\sum_{t=1}^{T} \boldsymbol{x}(t)\boldsymbol{x}^H(t) \tag{5}$$

where T is the number of training data samples. In (4), we can find that $\hat{\boldsymbol{R}}_v$ collects all the information on the sidelobe region, and the desired signal is removed. To calculate $\hat{\boldsymbol{R}}_v$, we uniformly sample u in U_s with M_s samples. (4) can be approximately calculated as

$$\hat{\boldsymbol{R}}_v = \sum_{i=1}^{M_s} \frac{\boldsymbol{a}(u_i)\boldsymbol{a}^H(u_i)}{f(u_i)}\Delta u \tag{6}$$

where $f(u_i) = \boldsymbol{a}^H(u_i)\hat{\boldsymbol{R}}_x^{-1}\boldsymbol{a}(u_i)$ which can be calculated by FFT (see Appendix).

Substituting the reconstructed covariance matrix $\hat{\boldsymbol{R}}_v$ (6) into the objective function (3a), we obtain

$$\boldsymbol{w}^H\hat{\boldsymbol{R}}_v\boldsymbol{w} = \sum_{i=1}^{M_s} g(u_i)|\boldsymbol{w}^H\boldsymbol{a}(u_i)|^2,\ u \in U_s \tag{7}$$

where $g(u_i) = \Delta u/f(u_i)$ which is the Capon spatial spectrum over the range U_s. It can be observed that the objective function can be obtained by the summation of weighted array power pattern associated with uniform sampling points over U_s. With consideration of the constraints (3b), minimizing the objective function (7) can be obtained by minimizing the sidelobe levels of the weighted power pattern where the weighting function is $g(u)$. However, the weighting function $g(u)$ is only defined in the siedelobe region U_s. We redefine

$$g(u) = \begin{cases} \Delta u/f(u),\ u \in U_s \\ \min\limits_{\varphi \in U_s} g(\varphi),\ u \in \overline{U}_s \end{cases}, \tag{8}$$

where $\overline{U}_s$ is the complement sector of U_s, i.e. $U_s \cup \overline{U}_s = [-1, 1]$. $\min\limits_{\varphi \in U_s} g(\varphi)$ means the smallest spectrum caused by white noise over region U_s. Therefore, the noise spatial spectrum in $\overline{U}_s$ will be no less than $g(u)$. When we consider the noise in the region $\overline{U}_s$, we can redefine the reconstructed interference-plus-noise covariance matrix (4) as

$$\hat{\boldsymbol{R}}_v = \int_{-1}^{1} \frac{g(u)}{\Delta u}\boldsymbol{a}(u)\boldsymbol{a}^H(u)\, du \tag{9}$$

Then (7) can be rewritten as

$$\boldsymbol{w}^H\hat{\boldsymbol{R}}_v\boldsymbol{w} = \sum_{i=1}^{M_s+M_m} g(u_i)|\boldsymbol{w}^H\boldsymbol{a}(u_i)|^2\ u_i \in [-1, 1] \tag{10}$$

where, $u_i \in \overline{U}_s$, $i = M_s+1,\ \ldots,\ M_s+M_m$. We point out that $g(u)$ is not the Capon spatial spectrum when $u \in \overline{U}_s$.

When u is uniformly sampled, the array pattern $\boldsymbol{P}$ can be evaluated by IFFT, where $\boldsymbol{P} = [\boldsymbol{w}^H\boldsymbol{a}(u_1),\ \ldots,\ \boldsymbol{w}^H\boldsymbol{a}(u_{Ms+Mm})]^T$. Here, we define a weighted array pattern $\boldsymbol{Q}$ which is given by

$$\boldsymbol{Q} = \boldsymbol{G} \bullet \boldsymbol{P} \tag{11}$$

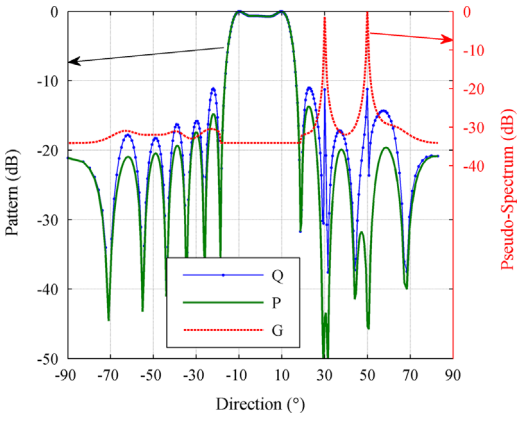

Fig. 1. The relationship among the weighted array pattern $\boldsymbol{Q}$, the array pattern $\boldsymbol{P}$, and the weighting function $\boldsymbol{G}$. Two interferences are at 30° and 50°. When the peak sidelobe level of $\boldsymbol{Q}$ is smaller than −10 dB, there are two deep nulls in $\boldsymbol{P}$ at 30° and 50°.

where $G = [\sqrt{g(u_1)}, \ldots, \sqrt{g(u_{Ms+Mm})}]^T$, the operation $\bullet$ represents the Hadamard product.

Now, we can transform problems (3a)–(3c) into a weighted pattern synthesis problem. That is to design a normalized pattern $\boldsymbol{Q}$ which satisfies:

a) The array gains in domain U_m are greater than a given value η.
b) The sidelobe levels are smaller than a prescribed level.

Here we give the reasons for these requirements. First, take the logarithm of $\boldsymbol{Q}$, $\boldsymbol{G}$, and $\boldsymbol{P}$ to get $\boldsymbol{Q}_{dB}$, $\boldsymbol{G}_{dB}$, and $\boldsymbol{P}_{dB}$, respectively. Then $\boldsymbol{Q}_{dB} = \boldsymbol{G}_{dB} + \boldsymbol{P}_{dB} + \alpha$, where $\alpha = 20\log(\max(\boldsymbol{G})\max(\boldsymbol{P})/\max(\boldsymbol{Q}))$ is a constant. As shown in Fig. 1, for restrictions (3b), when the values of $\boldsymbol{Q}_{dB}$ in the region U_m are greater than η, the values of $\boldsymbol{P}_{dB}$ in U_m will be greater than η too, because $\boldsymbol{G}_{dB}$ is constant over U_m. For constrains (3c), because the values of $\boldsymbol{G}_{dB}$ in U_s are equal to or greater than the values in U_m (see (8)), the sidelobe levels of $\boldsymbol{P}_{dB}$ will be not greater than ε as long as the values of $\boldsymbol{Q}_{dB}$ in U_s are not greater than ε. $\boldsymbol{G}_{dB}$ is the Capon spatial spectrum in the domain U_s, and there are peaks at the directions of interferences. Therefore, if the magnitudes of $\boldsymbol{Q}_{dB}$ at these directions are smaller than ε, the interferences are suppressed (nulls in $\boldsymbol{P}$, see Fig. 1).

In this paper, based on the Fourier transform-pair relationship between $\boldsymbol{w}$ and $\boldsymbol{P}$, we propose a modified iterative FFT based algorithm to solve it, which is described as

1) Calculate the vector $\boldsymbol{G}$.
2) Initialize the weights $\boldsymbol{w}$.
3) Apply a K ($K \geq M_s+M_m$) points IFFT to $\boldsymbol{w}$ by zero padding if necessary. The array pattern $\boldsymbol{P}$ is in the visible space.
4) Calculate the weighted array pattern $\boldsymbol{Q}$ with (11).
5) Adjust array pattern $\boldsymbol{P}$ according to the values of $\boldsymbol{Q}$. We want to design the weighted pattern $\boldsymbol{Q}$ to satisfy (a) and (b). If the $\boldsymbol{Q}$ does not satisfy the constraints, we need to adjust $\boldsymbol{Q}$ which is equal to adjust $\boldsymbol{P}$ (because $\boldsymbol{G}$ is unchanged during the iteration). For the sidelobe region,

find the points whose magnitudes in the weighted pattern $\boldsymbol{Q}$ are greater than the given levels, and then set the values of $\boldsymbol{P}$ associated with these points to be zeros. For the mainlobe region, adjust magnitudes of $\boldsymbol{P}$ corresponding to the points whose magnitudes in $\boldsymbol{Q}$ are smaller than the given level η to be greater values (For example $\eta+\Delta\eta$), and keep their phases unchanged.

6) Perform FFT to the adjusted pattern $\boldsymbol{P}$. Truncate the results to N samples to obtain the weights $\boldsymbol{w}$.
7) Iterate the steps (3)–(6) until the maximum number of iteration is reached or the desired pattern $\boldsymbol{Q}$ is arrived at.

Note that when the element spacing d is smaller than $\lambda/2$, $K>M_s+M_m$, otherwise, $K=M_s+M_m$. The array pattern $\boldsymbol{P}$ is in the visible space [24] of IFFT to $\boldsymbol{w}$. We have done a lot of simulation cases, and the maximum number of iteration is set to 80 which is large enough for a wide range of problem size (antenna number <50).

It is worthwhile noting that the proposed method is similar to the method in [14,16] that improves the robustness of the adaptive beamformer by adding magnitude response constraints in mainlobe [14,16] and sidelobe levels constraints [16]. However, the proposed approach introduced here is different from the method in [14,16], in the following aspects: (1) The method in [14,16] is to optimize the weights based on sample covariance matrix $\hat{\boldsymbol{R}}_x$, which tends to suppress the strong target signal to minimize the total output variance if the array model is not fully known [12,13]. However, the proposed method is to optimize the weights based on interference covariance plus noise covariance matrix $\hat{\boldsymbol{R}}_v$. When no model error exists, $\hat{\boldsymbol{R}}_v$ did not contain any information of the desired signal. Therefore, when we minimize (3a), the desired signal will not be affected. It is better to use $\hat{\boldsymbol{R}}_v$ than $\hat{\boldsymbol{R}}_x$ especially at high SNRs even when the model errors exist. (2) the method in [14,16] transforms problems (3a)–(3c) into a convex optimization problem which is solved by convex optimization algorithm directly. Due to this transformation, the number of unknown increases from N to $2N-1$, and more magnitude response constraints are required to imposed (equation (30e) of [14]). However, the proposed method just transforms the problem into a power pattern synthesis and an efficient iterative FFT based algorithm is applied to solve it. The computational complexity of the proposed method is mainly composed by the inverse of $\hat{\boldsymbol{R}}_x$ in (4) and the iterative processing. For each iteration, the computational complexity is about $O(K\log K)$. Therefore, the total computational complexity of the proposed method is $O(LK\log K+N^3)$, where L is the iteration number. The method in [14] has a complexity of $O(L_{IPM}(2N-1)^2(K+2N+1))$, where L_{IPM} (different from L in our method) is the number of iterations to solve the convex optimization problem by IPM method [14]. Moreover, the proposed method can choose a smaller K than the method in [14,16] do (see Section 3.4). Hence, the proposed method has complexity higher than the conventional Capon beamformer but lower than the method in [14,16] especially for large arrays.

Now we compare the proposed method and the method of [14] in operation counts and the computational time. The array element numbers choose as 15, 20, …, 55. The numbers of sampling point K are set as 90, 120, …, 330, respectively. The iteration number of our proposed method is set as 80. We suppose the iteration number of the method in [14] is 5 (actually, it may be greater than 5). The operation counts are given in Fig. 2. We also implement these two method in MATLAB on a laptop with an Intel Core i5-2430M with 4 GB RAM. To solve the convex problem in [14] we used CVX, a package for specifying and solving convex programs [26]. The computational time of these two methods are also shown in Fig. 2. We can find that the computational cost of the reference method increases quickly with the number of elements. Thanks to the application of FFT in our method, both operation counts and the computational time are much smaller than those of the reference method, especially for large arrays.

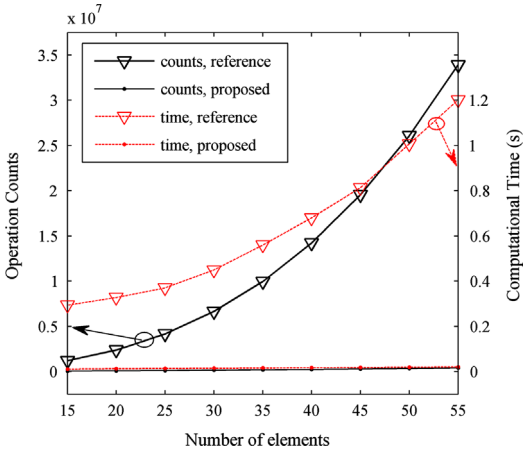

Fig. 2. The comparisons of the computational time and operation counts between the proposed method and the reference method in [4].

3. Simulation results

In this section, a uniform linear array with 16 isotropic antennas spaced a half wavelength apart is used. In all the simulations, the background noise is modeled as spatially and temporally independent complex Gaussian noise with zero mean and unit variance. Two interference sources are assumed to impinge on the array from 30° and 50°, unless it is specified otherwise. Both of them have signal power 20 dB. The desired signal is always presented in the training data and the SNR is assumed to be 20 dB unless it is specified otherwise. For each scenario, 200 Monte Carlo simulation runs are performed to obtain each simulated point. We will compare our proposed method with other state-of-the-art robust beamformers, including worst case based general rank beamformer (WC-GR) [6], Quadratically constrained beamformer (QC) [13], beamformer with constraints on magnitude response (CMR) [14], steering vector estimation beamformer (SVE) [10], and interference covariance matrix reconstruction based beamformer (ICMR) [12].

3.1. Example 1: Robust adaptive beamforming with different peak sidelobe levels

In this simulation case, we evaluate the proposed method with different desired sidelobe levels. The mainlobe area is $[-12^\circ, 12^\circ]$ (i.e. $U_m=[-0.21,0.21]$) and desired ripple level $\eta=0.93$. The desired peak sidelobe levels are set to -15 dB, -20 dB, -25 dB, -30 dB, and -35 dB, respectively. The sidelobe region is $U_s=[-1,-0.3]\cup[0.3,1]$. The target signal impinges on the array from 8° and the number of snapshots is 30. We set the maximum iteration number in our proposed method to be 40. The simulated array patterns are shown in Fig. 3. We can find out that all the array patterns are arrived at the desired peak sidelobe levels except SLL$=-35$ dB. That is because the peak sidelobes cannot arrive at that level with this mainlobe width restrictions even when no interference exists. Fig. 3(b) is a zoomed-in version of Fig. 3(a) around the interference directions. As shown in Fig. 3(b), the array magnitudes at 30° and 50° are small for all the desired peak sidelobe level settings. However, there is no trough at the interference direction when SLL$=-35$ dB. Because the array takes more effort to decrease the sidelobe levels other than to suppress the interference. High sidelobes can lower the tolerance to white noise and moving interferences. If we set a relative higher desired peak sidelobe level, we can expect deeper nulls at the directions of interferences. In real world applications, if the power of interference is very high, one may want to set a higher desired PSLL; if the direction of interferences change too fast, one need to set a lower desired PSLL.

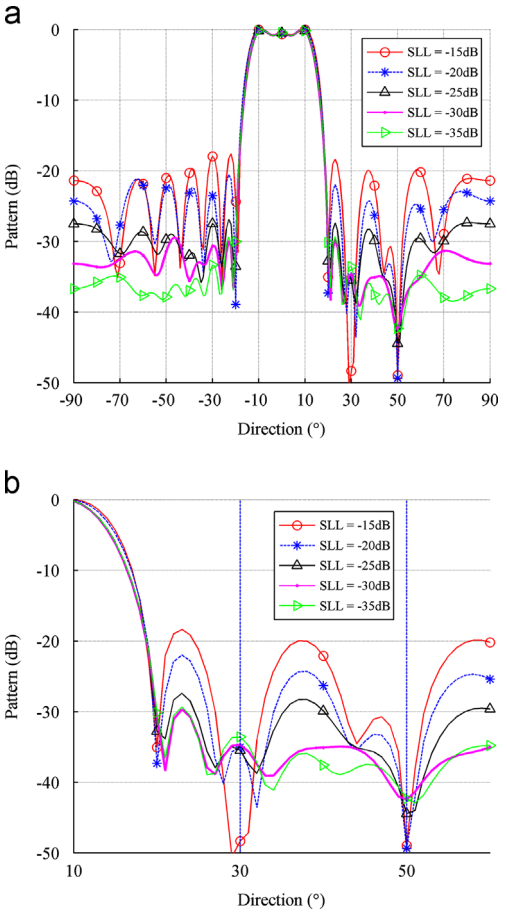

Fig. 3. Example 1: the proposed beamformer with different desired PSLLs. (a) the array patterns for different desired PSLLs; and (b) zoomed-in patterns.

3.2. Example 2: Robust adaptive beamforming with different beamwidths

The proposed method can design an adaptive beamformer with a given beamwidth. The beamwidths are set to 4°, 12°, 20°, 28° (i.e. $U_m=[-0.035, 0.035]$, $[-0.105, 0.105]$, $[-0.175, 0.175]$, $[-0.247, 0.247]$, respectively). The desired peak sidelobe level is -20 dB for all the four cases and the desired ripple level $\eta=0.93$. As shown in Fig. 4, the proposed method can obtain the array pattern with different beamwidths and the same nulls at 30° and 50°. A wider beamwidth can improve the robustness of the beamformer against steering vector errors. However, a wider beamwidth means the beamformer degrades the ability to get deep nulls and receives more noise from the mainlobe that will decrease the output SINR. For example, when the target signal comes from 0° (SNR$=-20$ dB), the output SINRs associated with beamwidths 4°, 12°, 20°, 28° are -8.3 dB, -12.2 dB, -13.3 dB, and -14.9 dB, respectively. Here, the optimal SINR is equal to -8 dB. We also can design beamformers with different mainlobe ripple levels. We point out that if there is a interference closing to the desired signal, this interference may locate at mainlobe region when the beamwidth is wide. Therefore, the interference cannot be suppressed.

3.3. Example 3: Robust adaptive beamforming with a moving target signal

If the target signal is moving too fast, the adaptive beamforming weights should be updated quickly. This will increase computational cost. In this simulation, we will consider this practical application with the proposed method. We suppose the target signal impinges on the array from 0° (20 dB), and the angular velocity of this

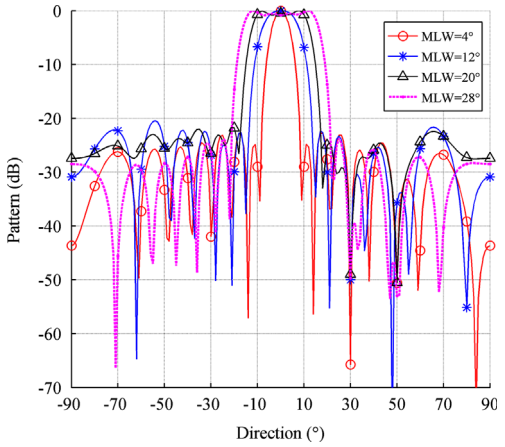

Fig. 4. Example 2: array pattern with different beamwidths.

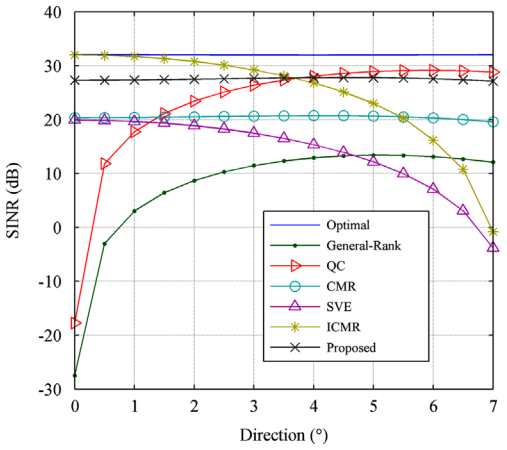

Fig. 5. Example 3: the performance of different beamformers with moving target signals.

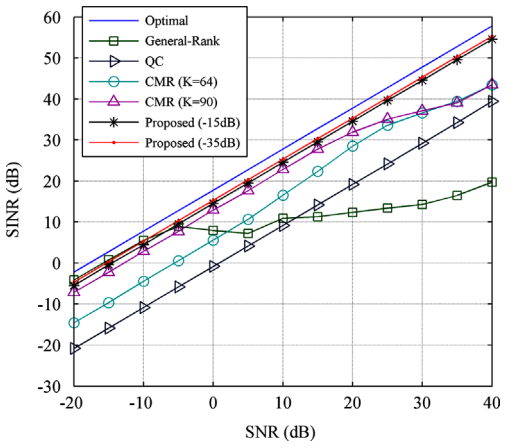

Fig. 6. Example 4: the output SINR versus SNR for different beamforming methods.

target is 1° per second. The weights is calculated by using the data received in the first second. All the methods will not adapt their weights in the next seven seconds and apply the weights calculated by training data as the "frozen weights". Now we consider the output SINRs in the following each second which means when the target moves to 1°, 2°, …, 7°, respectively. For the beamformers WC-GR [6], QC [13], CMR [14], and the proposed method, we set the robust mainlobe region equal to $[-7°, 7°]$. According to the Lemma 1 in [13], QC beamfomer cannot obtain a pattern whose beamwidth is greater than $2\times\arcsin(\lambda/2Nd)$. Therefore, there is an unavoidable null in the mainlobe region $[-7°, 7°]$ with QC beamformer. As shown in Fig. 5, the same phenomenon can be found in the WC-GR beamformer. The CMR beamformer and the proposed beamformer both can obtain a flat-top beampattern which means the beamformers have nearly constant output SINRs as the target moves. However, SVE beamformer [10] and ICMR beamformer [12] degrade their performance rapidly as the target moves away from 0°. Compared with SVE and ICMR, the proposed method is more robust against moving target signals at the cost of the ability of noise suppression. Therefore, we can find that the SINR of ICMR beamformer is higher than that of the proposed method at DOA range [0°, 3°]. We point out that if the mainlobe region is chosen as [0°, 7°], WC-GR beamformer and QC beamformer can give nearly constant output SINRs as target moves from 0° to 7°.

3.4. Example 4: Robust adaptive beamforming with locally incoherent scattered target signals

This example corresponds to the scenario where the target signal is distorted by the incoherent local scattering effect. The signal is assumed to have time-varying spatial signature that is different for each snapshot and the actual steering vector is formed by five incoherent paths:

$$\overline{\boldsymbol{a}} = s_0(t)\boldsymbol{a}(u_0)+\sum_{i=1}^{4} s_i(t)\boldsymbol{a}(u_i) \quad (12)$$

where $s_i(t)$, $i=0,1,\ldots,4$ are independently and identically distributed complex Gaussian random variable with zero-mean and unit variance, $u_i=\sin(\theta_i)$, θ_i are independently drawn in each simulation run uniformly from $[-5°,5°]$. The DOAs of two interferences in this example are randomly chosen in the sidelobe area $([-90°,-12°]\cup[12°,90°])$, and their power are both 20 dB. In our proposed method, the beamwidth is assumed to be 10° and the ripple level in the mainlobe is $\eta=0.93$. The desired peak sidelobe level is set to two different values, -15 dB and -35 dB. The number of samples K in angular domain in our proposed method is assumed to be 64 and the iteration number is set to 40. In each simulation run, the DOAs of θ_i and interferences are all random chosen. After 200 Monte Carlo simulations, the simulation results are shown in Fig. 6. Although the obtained pattern cannot arrive at the global optimal one within 40 iterations in most simulation runs, the output SINRs of the proposed method are still better than its competitors. The SINRs of PSLL$=-35$ dB are a little higher than that of PSLL$=-15$ dB because lower sidelobes have higher tolerance to white noise. As described in Section 2, the CMR beamformer in [14] is sensitive to the number of samples K. If K is chosen too small, the optimized $\boldsymbol{r}$ may not be an autocorrelation sequence of $\boldsymbol{w}$. As shown in Fig. 6, the performance of CMR with $K=90$ is better than that of CMR with $K=64$. However, the proposed method can obtain good results when $K=64$. Due to the desired beamwidth is greater than $2\times\arcsin(\lambda/2Nd)$, the output SINRs of the QC beamformer are low over the range of SNRs.

3.5. Example 5: Robust adaptive beamforming with element position errors

The robust adaptive beamformers will degrade in the presence of steering vector errors. One common source of error comes from the error in the knowledge of the antenna array geometry. Here, in each simulation run, we assume the element position errors are drawn uniformly from $[-\alpha, \alpha]$, where α is the level of perturbations which is measured in wavelengths. The target signal is impinging on the array from 3° with SNR$=20$ dB. We restrict the mainlobe beam in

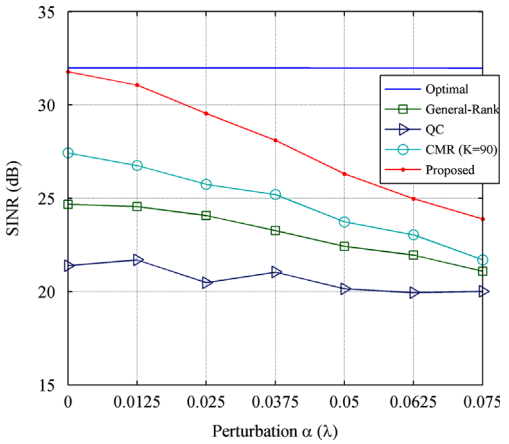

Fig. 7. Example 5: the output SINRs versus different element position perturbation levels.

[0°, 5°]. With this beamwidth choice, QC beamformer can obtain a pattern with nearly constant magnitude over the range. In the proposed method, the desired PSLL is chosen as -15 dB. The comparison of performance of different beamformers versus different perturbation levels is shown in Fig. 7. The output SINR, of the proposed method and CMR method decreases as the increases of α. Because the element position error will affect null steering in the pattern synthesis process. However, QC beamformer has nearly constant output SINRs, because the performance of QC is only related to the error of steering vector associated with the target signal and the steering vector error has little effect on null steering. Although the QC method has better robustness against the element position errors, the proposed method still outperforms other methods (including QC method) even when the perturbation α is as large as 0.075λ (i.e. 15% of element spacing).

4. Conclusion

In this paper, we proposed a robust adaptive beamforming method with beampattern shaping constraints. The main idea is transforming the adaptive beamforming problem into a pattern synthesis problem. The constraint of constant magnitude response in the mainlobe is a nonconvex problem which can be solved by a proposed iterative FFT method. The iterative FFT method cannot guarantee the global optimal weights can be found in the pattern synthesis process. However, as shown in the Section 3, the local optimal weights can also give good results for adaptive beamforming.

Acknowledgments

This work was supported in part by the National Natural Science Foundation of China under Grants 61032010 and 61171044, in part by the Fundamental Research Funds for the Central Universities.

Appendix

Calculate $f(u)$ by FFT:

$$f(u_i) = a^H(u_i)\hat{\boldsymbol{R}}_x^{-1}a(u_i)$$
$$= \sum_{m=1}^{N}\sum_{n=1}^{N}\hat{\boldsymbol{R}}_x^{-1}(m,n)e^{j2\pi d(n-m)u_i/\lambda}$$
$$= \sum_{n=-N+1}^{N-1} r_n e^{j2\pi dnu_i/\lambda}$$

where, $r_n = \sum_{1\le m\le N;\ 1\le m+n\le N}\hat{\boldsymbol{R}}_x^{-1}(m,\ m+n)$. When u_i is uniformly sampled, $f(u_i)$ can be calculated by fast Fourier transform.

References

[1] J.E. Hudson, Adaptive Array Principles, Peregrinus, UK, 1981.
[2] D.D. Feldman, L.J. Griffiths, A projection approach to robust adaptive beamforming, IEEE Transactions on Signal Processing 42 (1994) 867–876.
[3] J. Li, P. Stoica (Eds.), Wiley, New York, 2006.
[4] S. Vorobyov, A.B. Gershman, Z.Q. Luo, Robust adaptive beamforming using worst-case performance optimization: a solution to the signal mismatch problem, IEEE Transactions on Signal Processing 51 (2003) 313–324.
[5] F. Huang, W.X. Sheng, X.F. Ma, W. Wang, Robust adaptive beamforming for large-scale arrays, Signal Processing 90 (2010) 165–172.
[6] S. Shahbazpanahi, A.B. Gershman, Z.Q. Luo, K.M. Wong, Robust adaptive beamforming for general-rank signal models, IEEE Transactions on Signal Processing 51 (2003) 2257–2269.
[7] W. Zhang, J. Wang, S. Wu, Robust Capon beamforming against large DOA mismatch, Signal Processing 93 (2013) 804–810.
[8] J. Li, P. Stoica, Z. Wang, On robust Capon beamforming and diagonal loading, IEEE Transactions on Signal Processing 51 (2003) 1702–1715.
[9] F. Huang, W.X. Sheng, X.F. Ma, Modified projection approach for robust adaptive array beamforming, Signal Processing 92 (2012) 1758–1763.
[10] A. Khabbazibasmenj, S.A. Vorobyov, A. Hassanien, Robust adaptive beamforming based on steering vector estimation with as little as possible prior information, IEEE Transactions on Signal Processing 60 (2012) 2974–2987.
[11] Y.J. Gu, W.P. Zhu, M.N.S. Swamy, Adaptive beamforming with joint robustness against covariance matrix uncertainty and signal steering vector mismatch, Electronics Letters 46 (2010) 86–88.
[12] Y.J. Gu, A. Leshem, Robust adaptive beamforming based on interference covariance matrix reconstruction and steering vector estimation, IEEE Transactions on Signal Processing 60 (2012) 3881–3885.
[13] C.Y. Chen, P.P. Vaidyanathan, Quadratically constrained beamforming robust against direction-of-arrival mismatch, IEEE Transactions on Signal Processing 55 (2007) 4139–4150.
[14] Z.L. Yu, W. Ser, M.H. Er, Z. Gu, Y. Li, Robust adaptive beamformers based on worst-case optimization and constraints on magnitude response, IEEE Transactions on Signal Processing 57 (2009) 2615–2628.
[15] Z.L. Yu, Z. Gu, J. Zhou, Y. Li, W. Ser, M.H. Er, A robust adaptive beamformer based on worst-case semi-definite programming, IEEE Transactions on Signal Processing 58 (2010) 5914–5919.
[16] S.E. Nai, W. Ser, Z.L. Yu, S. Rahardja, A robust adaptive beamforming framework with beampattern shapping constraints, IEEE Transactions on Antennas and Propagation 57 (2009) 2198–2203.
[17] S.E. Nai, W. Ser, Z.L. Yu, H. Chen, Iterative robust minimum variance beamforming, IEEE Transactions on Signal Processing 59 (2011) 1601–1611.
[18] J. Liu, A.B. Gershman, Z.Q. Luo, K.M. Wong, Adaptive Beamforming with sidelobe control: a second-order cone programming approach, IEEE Signal Processing Letters 10 (2003) 331–334.
[19] L. Zhang, W. Liu, R.J. Langley, A class of constrained adaptive beamforming algorithms based on uniform linear arrays, IEEE Transactions on Signal Processing 58 (2010) 3916–3922.
[20] A. De Maio, S. De Nicola, A. Farina, S. Iommelli, Adaptive detection of a signal with angle uncertainty, IET Radar, Sonar and Navigation 4 (2010) 537–547.
[21] A. De Maio, Y. Huang, M. Piezzo, S. Zhang, F. Alfonso, Design of optimized radar codes with a peak to average power ratio constraint, IEEE Transactions on Signal Processing 59 (2011) 2683–2697.

[22] W.P.M.N. Keizer, Fast low-sidelobe synthesis for large planar array antennas utilizing successive fast Fourier transforms of the array factor, IEEE Transactions on Antennas and Propagation 55 (2007) 715–722.
[23] W.P.M.N. Keizer, Element failure correction for a large monopulse phase array antenna with active amplitude weighting, IEEE Transactions on Antennas and Propagation 55 (2007) 2211–2218.
[24] K. Yang, Z. Zhao, Q.H. Liu, Fast pencil beam pattern synthesis of large unequally spaced antenna arrays, IEEE Transactions on Antennas and Propagation 61 (2013) 627–634.
[25] K. Yang, Z. Zhao, Q.H. Liu, An iterative FFT based flat-top footprint pattern synthesis method with planar array, Journal of Electromagn, Waves and Applications 26 (2012) 1956–1966.
[26] M. Grant, S. Boyd, CVX: Matlab software for disciplined convex programming, ⟨http://cvxr.com/cvx⟩, 2012.